THE JOURNAL OF PHYSICAL CHEMISTRY C

Article

pubs.acs.org/JPCC

NO Adsorption on Copper Phthalocyanine Functionalized Graphite

Jun Hong Park,[†,‡] Pabitra Choudhury,[§] and Andrew C. Kummel*[,‡]

[†]Materials Science & Engineering Program and [‡]Departments of Chemistry & Biochemistry, University of California, San Diego and La Jolla, California 92093, United States

[§]Department of Chemical Engineering, New Mexico Tech, Socorro, New Mexico 87801, United States

Supporting Information

ABSTRACT: NO dosed on a CuPc monolayer deposited on Au(111) and HOPG is observed by scanning tunneling microscopy. After dosing NO with a supersonic molecular beam source onto CuPc/Au(111), about 7% of CuPc molecules form chemisorbates with NO. Conversely, after dosing onto CuPc/HOPG, only about 0.1% CuPc molecules form chemisorbates with NO, even though the reaction sites appear nearly identical. DFT calculations were employed to elucidate the mechanism which causes the >10× difference in saturation coverage between NO/CuPc/Au(111) and NO/CuPc/HOPG. DFT calculations show NO chemisorption with CuPc/Au(111) induces only negligible perturbation in the density of states (DOS) in Au(111) due to large density of states on Au. Conversely, for NO/CuPc/HOPG, there is a large decrease of DOS in graphene around 1 eV due to NO chemisorption on CuPc/graphene consistent with negative charge transfer from graphene to NO. This DOS perturbation of graphene results in decreased binding energy of NO chemisorption in secondary NO sites, consistent with low saturation coverage. The results suggest that although the saturation coverage of NO chemisorbates is low on CuPc/graphene, the DOS of graphene can be altered by low coverages of adsorbates even onto weakly interacting molecules which chemically functionalize the graphene surface.

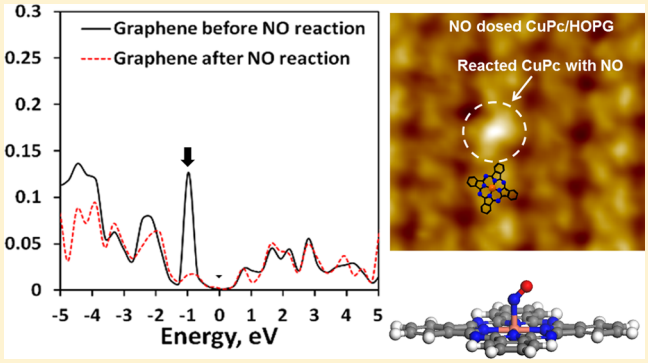

INTRODUCTION

Graphene, a 2D semiconductor material, consists of sp^2 bonded carbon atoms in a honeycomb lattice forming a single layer.[1] Graphene has high carrier mobility as well as a chemically and electronically passivated surface, thereby rendering graphene to be a promising electronic material for novel devices.[2−5] Graphene also has potential for chemical sensing platforms, due to its atomically thin body.[6,7] The atomically thin body of graphene allows each carbon atom to directly interact with ambient analytes, thereby increasing chemical sensitivity. However, the surface of graphene is chemically inert, thereby requiring modification for use in electronic and sensor devices.[8−10] One common approach is oxidation of graphene with chemical reduction, but this oxidation also involves introduction of defects.[11−13] An effective strategy to modify the chemical sensitivity of graphene is functionalization with other materials without perturbing the graphene electronic structure. For example, a self-assembly layer by organic molecules can be effective for fabrication of graphene based chemical or bio sensors.[14−16]

Metal phthalocyanines (MPc) may enhance the sensing performance of graphene chemical sensors via functionalization. MPc have been widely studied as chemical sensors.[17−22] The MPc films can be deposited to form well-ordered layers on inorganic substrates, including graphene or graphite surfaces.[23−27] Moreover, MPcs can maintain their molecular structure at high temperature and only a few acids are able to decompose MPcs. MPc molecules have delocalized π-electrons, enabling them to act as electron donors, thereby providing a low activation energy for formation of charge transfer complexes with oxidizing analytes in chemical sensing.[17,28,29]

MPc detection of chemical analytes is induced primarily by charge transfer reactions between the central metal ion and analytes; therefore, in a simplified model, the analytes act as MPc "dopants":[30,31] Pure MPcs films of organic thin film transistor (OTFT) in vacuum have a Fermi level in the middle of the band gap. However, when MPcs films are exposed to oxidative agents, MPc become p-type semiconductors.[17,30−32] The induced p-type conductivity of MPc films has been modeled as formation of charge transfer complexes on the metal centers with oxidative analytes. Oxidative analytes (such as O_2),[20,31] which are electron acceptors, chemisorb on MPc molecules, forming superoxide adducts consisting of oxidized MPc^+ and O^{2-} species. During this reaction, electrons are transferred from MPc to analytes. Simultaneously, holes are injected into the MPc molecules to form positively charged MPc^+. The injection of these holes moves the HOMO edge toward the Fermi level forming a p-type MPc film.[17] Due to

Received: January 8, 2014
Revised: April 19, 2014
Published: April 22, 2014

   dx.doi.org/10.1021/jp5002258 | J. Phys. Chem. C 2014, 118, 10076−10082

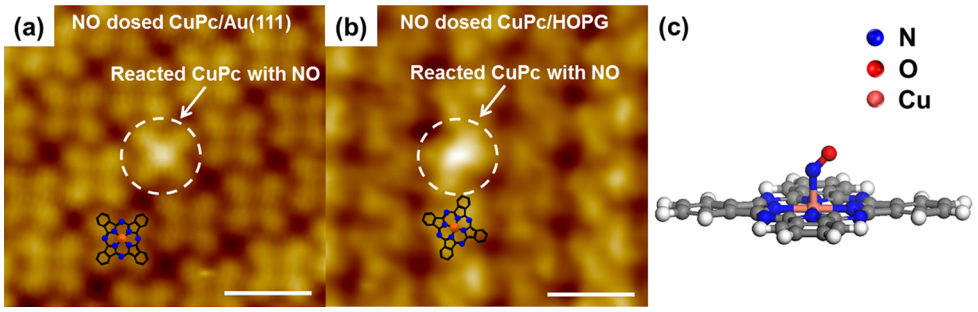

Figure 1. Submolecular resolution empty state STM images of a CuPc monolayer surface dosed with NO on Au(111) and HOPG at 150 K. Diluted NO was dosed by MBS, and nozzle was held at 300 K. Empty state STM images were recorded with V^s = +2.0 V, I_t = 20 pA. The pulsing of the MBS was 30 Hz with 100 μs opening time. Scale bars indicate 2 nm. The reacted sites are denoted by circles. (a) Submolecular resolution of CuPc chemisorbed with single NO molecule on Au(111). The center of CuPc is modified into bright spot. (b) Submolecular resolution of CuPc chemisorbed with single NO molecule on HOPG. The center of CuPc is modified into bright spot. (c) Chemisorption model of NO with CuPc.

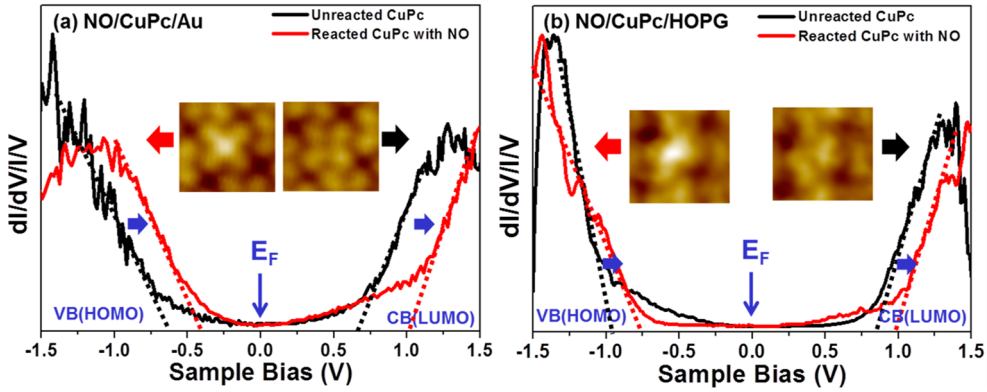

Figure 2. Scanning tunneling spectroscopy (STS) dI/dV curves of unreacted and reacted CuPc molecules. All spectra recorded at the center of the CuPc and were swept from −2 to 2 V. (a) STS dI/dV spectra of NO/CuPc/Au(111). (b) STS dI/dV spectra of NO/CuPc/HOPG. The black spectra indicate STS from unreacted CuPc molecules, while red spectra show STS from CuPc molecules with chemisorbed NO. After NO chemisorption on CuPc molecules, the E_F was shifted toward the VB (HOMO) in both NO/CuPc/Au(111) and NO/CuPc/HOPG.

these properties and MPc adsorption on graphene not perturbing its atomic structure, MPc molecules are suitable to functionalize graphene for chemical sensing.

The present study employs molecular scale imaging and tunneling spectroscopy to investigate NO adsorption on copper phthalocyanine (CuPc) monolayers deposited on highly oriented pyrolytic graphite (HOPG). The HOPG surface has similar electronic properties to graphene, including a nearly inert surface and a zero band gap. NO also was dosed onto CuPc/Au(111) for comparison with NO/CuPc/HOPG. Using STM, the dependence of NO absorption on the MPc support (HOPG vs Au(111)) was elucidated. To understand the electronic changes of the HOPG surface induced by generation of NO/CuPc/HOPG complexes, DFT calculations were performed.

EXPERIMENTAL SECTION

All experiments were performed in a commercial multichamber Omicron ultrahigh vacuum (UHV) system with a base pressure below 1 × 10^{-10} Torr. Clean Au(111) and HOPG surfaces were prepared as substrates for CuPc deposition. The surface of a single crystal Au(111) was cleaned by multiple sputtering cycles with a 0.5 to 1 kV of Ar+ ion beam (RBD instruments) with an Ar background pressure of 6 × 10^{-5} Torr at 300 K surface temperature. After sputtering, the Au(111) sample was annealed at 773 K for 30 min. This sputtering and annealing cycle was repeated until an atomically flat Au(111) surface was obtained in STM imaging. The Highly Ordered Pyrolytic Graphite (HOPG) substrate was cleaved in air before being loaded into the vacuum chamber. Afterward, the cleaved HOPG sample was annealed at 823 K for 5 h to obtain large, flat and clean areas as shown in the STM imaging.

The CuPc was purchased from Sigma-Aldrich and purified by multiple sublimation cycles. The CuPc monolayer sample was deposited as thick overlayers of CuPc on clean Au(111) and HOPG surfaces by organic molecular beam epitaxy with a differentially pumped effusion cell (Eberl MBE- Komponenten), while the sample was in the UHV preparation chamber, as shown in Suppoting Information, SI, Figure S1. During deposition, both the Au(111) and HOPG were held at 373 K. Subsequently, the CuPc multilayers on Au(111) were heated to 623 K for 4 min to form a flat-lying monolayer of CuPc on the Au(111) observed by in situ STM, because the CuPc/CuPc interactions in multilayers are weaker than the CuPc/Au(111) surface interaction.[33] Conversely, the CuPc multilayer on HOPG was annealed at 473 K for 6 min surface to form a flat-lying monolayer of CuPc on the HOPG observed by in situ STM. This lower annealing temperature on HOPG results from the weaker interaction CuPc with HOPG than with Au(111).

NO was dosed on CuPc monolayer in the UHV chamber at 150 K with use of a pulsed supersonic molecular beam source (General Valve Series 1), which was differentially pumped using a three chamber differentially pumped source with turbomolecular pumps (TMP). The NO analyte was diluted in He (He:

dx.doi.org/10.1021/jp5002258 | J. Phys. Chem. C 2014, 118, 10076−10082

95%; NO: 5%). The low surface temperature was employed so that the chemisorbate would be stable on the surface for STM Imaging. The pulsed molecular beam operated at 30 Hz with a 100 μs opening time. Note this the supersonic molecular beam source will produce a nearly monoenergetic beam of NO with an approximate translational energy of 0.33 eV, so it slightly favors direct chemisorption over precursor chemisorption compared to a thermal gas source at 300 K.[34] Before flowing, the diluted NO gas with pulsed valve into preparation chamber, the preparation chamber was pumped only with a turbomolecular pump (TMP) and held at 1×10^{-9} Torr. Upon activating the pulsed NO/He beam, the pressure rose to 2×10^{-7} Torr. The dosing time was 10 min for the data in Figures 1, 2, and 3. After dosing the NO, the samples were transferred immediately to an STM chamber; the sample stage on the STM was maintained at 100 K to minimize analyte desorption. All STM work was performed at $<5 \times 10^{-11}$ Torr, and all STM images were acquired using electrochemically etched W tips.

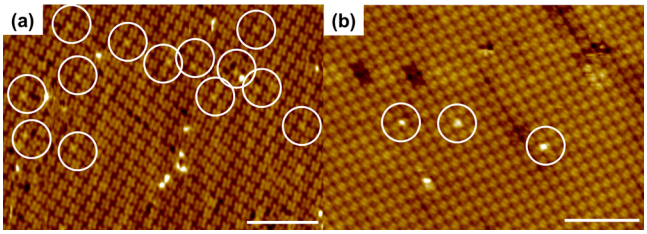

Figure 3. Empty-state STM images of a CuPc monolayer surface dosed with NO on Au(111) and HOPG. STM images were recorded with V_s = 2.0 V, I_t = 20 pA. Scale bars indicate 10 nm. The white circles indicate CuPc molecules with chemisorbed NO. (a) CuPc monolayer dosed NO for 10 min on Au(111). About 7% of CuPc molecules reacted with NO on CuPc/Au(111). (b) CuPc monolayer dosed NO for 10 min on HOPG. Approximately 0.1% of CuPc molecules reacted with NO on CuPc/HOPG. The coverage of saturation NO coverage is much smaller on HOPG than on Au(111).

RESULTS AND DISCUSSION

The CuPc monolayer/Au(111) dosed with NO was imaged in UHV-STM to observe the change induced by NO dosing. All imaging was performed at V_s = 2 V. As shown in an empty state STM image of Figure 1, NO chemisorption on a CuPc monolayer/Au(111) at 150 K results in topographic modification of the Cu atom which is located at the center of CuPc molecule. The molecular structure of CuPc is clearly defined in a submolecular resolution STM image in Figure 1 (a). While the outer carbon aromatic rings have 4-fold symmetry and are bright in STM imaging, the unreacted Cu^{2+} is located in center of the molecule and appears as dark hole. After chemisorption of NO, the topographic appearance of core Cu atom is modified into a bright protrusion, while the 4-leaf pattern of ring remains. This modified bright symmetric protrusion, which appears in the center of CuPc, is consistent with a single NO molecules binding to the Cu atom of CuPc.

NO chemisorbates are also observed on CuPc/HOPG, as shown in Figure 1(b). The topographic appearance of these chemisorption sites to similar NO/CuPc on Au(111); a dark hole, which assigned to Cu, is modified into symmetric bright spot. It has previously been shown by DFT calculations that NO binding with Cu via the N terminal of NO has the highest stability and the Cu−N−O bond is bent in Figure 1(b).[35] However, STM images do not show observable bending or tilting of NO binding consistent with the bound NO continuously rotating on Cu ion because NO has a single bond to Cu. A schematic binding configuration of NO with CuPc molecules is presented in Figure 1(c).

Scanning tunneling spectroscopy (STS) was employed to investigate the changes in the electronic structure of CuPc/Au(111) and CuPc/HOPG due to NO chemisorption, as shown in Figure 2. It is noted that all dI/dV curves were measured on central area of the CuPc molecules, and swept from −2 to 2 V. During measurement all spectra, STM tips were approached to surface (Δz = ∼0.1 nm) for detecting larger tunneling signal. Although thick CuPc films have a 2.3 eV band gap,[36,37] the measured band gaps of CuPc molecules on Au(111) and HOPG are much smaller; 1.5 eV for NO/CuPc/Au(111) and 1.75 eV for NO/CuPc/HOPG. The difference in band gap between these two systems is consistent with the difference in the density of states (DOS) between Au(111) and HOPG. During STS measurements on CuPc molecules, the STM tips measure tunneling currents not only from CuPc molecules, but also from the Au(111) or HOPG surfaces because the metal tips are within a few angstroms of Au(111) or HOPG.[38] Both Au(111) and HOPG have metallic or semimetallic density of states as shown by their zero band gaps in STS, but the Au(111) surface has larger density of states than HOPG. The measured DOS of substrates is mixed with DOS of CuPc, so a narrower band gap appears in STS curves for NO/CuPc/Au(111) than for NO/CuPc/HOPG.

The STS of the clean CuPc molecules on Au(111) and HOPG shows the Fermi level (E_F, 0 V position in STS) in the middle of the band gap (black curves) shown in Figure 2, both parts (a) and (b). Unreacted CuPc (black line) has a Fermi level (E_F) almost in the middle of the band gap on both of Au(111) and HOPG. The CuPc monolayer has almost zero conductance from −0.5 to 0.5 V, and this zero conductance appears as the band gap. This band gap indicates that unreacted CuPc molecules act as intrinsic semiconductor in vacuum.

After NO chemisorption onto CuPc molecules, the Fermi level of CuPc molecules is shifted toward the valence band, which corresponds in a molecule to the highest occupied molecular orbital (HOMO) of CuPc on both Au(111) and HOPG, as shown in Figure 2. For NO/CuPc chemisorbates on Au(111) surface, the E_F shift (blue arrow) is about 0.3 eV (Figure 2(a)). This shift of Fermi level is also observed in NO/CuPc/HOPG, as shown in Figure 2(b). After NO chemisorption on metal center of CuPc, the Fermi level moves about 0.25 eV toward the HOMO. However, these NO induced E_F shifts on both Au(111) and HOPG might not be denoted as "p-doping", but instead are denoted here as dipole-induced shifts because the Fermi are still in the band gap on both Au(111) and HOPG. It is noted these shift are consistent with CuPc being a net charge donor during reaction with NO on both substrates.

Although NO chemisorption on CuPc induces Fermi level shifts on both Au(111) and HOPG, the CuPc layers show large differences in saturation NO coverage. After dosing NO from the MBS at 30 Hz with 100 μs opening time for 10 min at 150 K, STM images reveals ∼7% of CuPc molecules/Au(111) are reacted with NO and form NO chemisorbates in Figure 3(a). The dose corresponds to a saturation dose since increasing the dose time twofold did not create more chemisorption sites. It is estimated that the dose corresponds to ∼30 L per each Au atom, since the pressure rise in the chamber was 2×10^{-7} Torr for 600 s, and a background almost entirely of NO, since the

dx.doi.org/10.1021/jp5002258 | J. Phys. Chem. C 2014, 118, 10076−10082

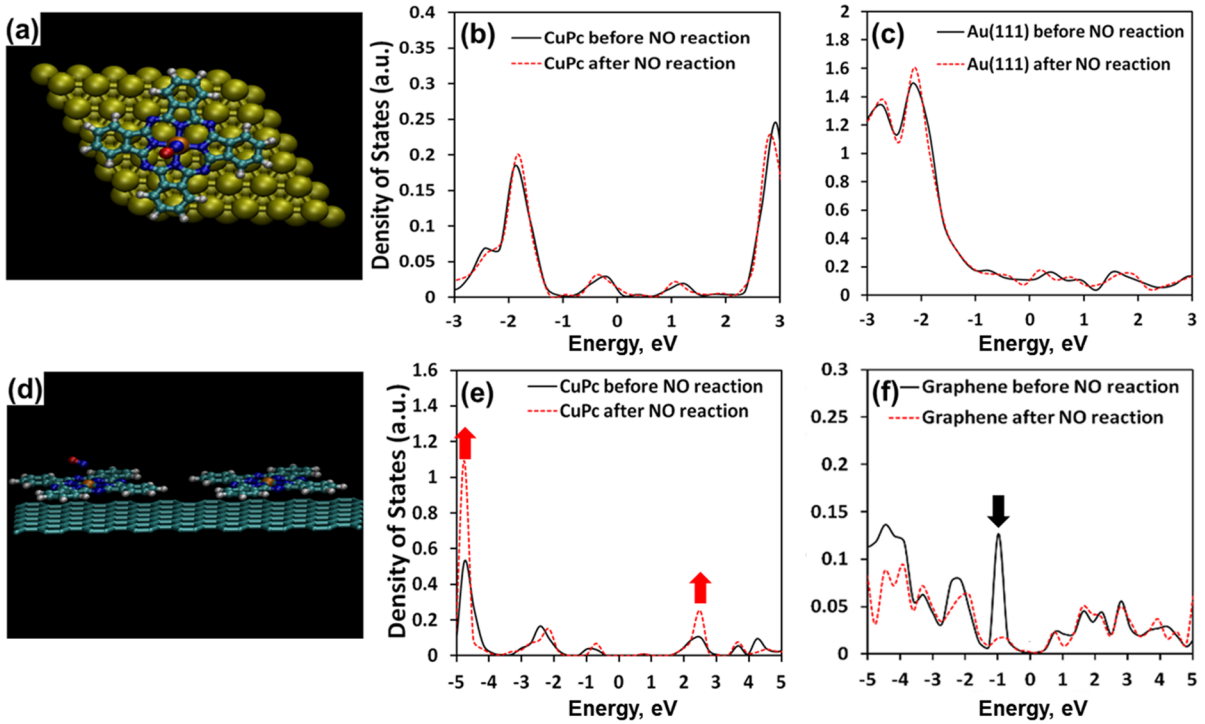

Figure 4. Density Functional Theory models of NO/CuPc/Au(111) and NO/CuPc/graphene. (a) Binding configuration of NO chemisorption site on CuPc/Au(111). (b),(c) Projected density of states of CuPc molecules and Au(111) before and after NO binding on CuPc/Au(111). (d) Binding configuration of NO chemisorption site on CuPc/HOPG. (e),(f) Projected density states of CuPc molecules and graphene before and after NO binding on CuPc/graphene. The NO adsorption induces a decrease of graphene DOS at 1 eV below the Fermi surface (black arrow) in the valence band, while increasing the DOS of CuPc near 4.5 eV below the Fermi surface and 2.5 eV above the Fermi surface in the conduction band (red arrow). The Fermi surface is shifted to zero level on the *x*-axis in the plots.

pressure gauge is insensitive to He and because heavy molecules are concentrated to centerline during expansion in the supersonic nozzle of MBS.[34] These NO chemisorbates are dispersed, i.e., island formation is not observed. After exposing NO of equivalent dosage (10 min) on CuPc monolayer deposited on HOPG at 150 K, NO dosing also induces saturation coverage of NO on CuPc/HOPG, but the saturation coverage of NO is much smaller (~0.1%) on HOPG than on Au(111). Only few CuPc molecules react with NO and form NO chemisorbates in Figure 3(b).

Although NO chemisorbates can be detected on both Au(111) and HOPG surfaces, charge transfer behavior is different on each surface. Charge transfer can occur between the CuPc monolayer and substrates. When CuPc molecules monolayers are formed on Au, electron charge is transferred from the CuPc molecules to the Au(111) surface due to band alignment at CuPc/Au(111) interface.[39−42] Metal phthalocyanines have nonuniform charge distribution.[43,44] A previous report showed that charge can be transferred from the nitrogen atoms of CuPc molecules to Au(111) surface via the central Cu ion.[41] For HOPG, the top layer of HOPG does not have dangling bonds and adsorbates only have weak van der Waals interactions with the π orbitals.[45] Therefore, when CuPc molecules are deposited on HOPG, the delocalized π electrons of CuPc form just a weak $\pi-\pi$ van der Waals interaction with HOPG. Furthermore, since E_{vac} (vacuum level) of CuPc is nearly same with HOPG, very small charge transfer occurs between CuPc and HOPG.[45−49] As shown below in the detailed DFT calculations, these factors are a small effect since the binding energy of isolated NO molecule on CuPc is independent of the substrate; instead, it is the difference in density of states of the substrate which determines the difference in saturation coverage.

Density of functional theory calculations were performed to understand the differences in NO chemisorption and charge transfer for NO/CuPc/Au(111) and NO/CuPc/HOPG, as shown in Figure 4 and SI Figures S2 and S3 as a complement to the experiments. The Vienna Ab Initio Simulation Package (VASP) was employed to calculate van der Waals corrected spin-polarized periodic DFT.[50−54] For NO on CuPc/Au(111), which has binding energy −0.24 eV in Figure 4(a), the density of states (DOS) of Au(111) shows almost no change upon NO chemisorption even though NO loses electron charge (0.07 e) to CuPc/Au(111). As shown in Figure 4, parts (b) and (c), initially, Au(111) accepts 0.08 electrons from adsorbate-free CuPc; after NO chemisorption, Au(111) accepts 0.19 electrons from NO and CuPc. Thus, there is an excess 0.11 electrons transferred to Au(111) surface. Out of total 0.19 electrons transferred to Au(111) surface, only 0.07 electrons comes from NO (see SI Figure S2) and the remaining 0.12 electrons transfer from CuPc during NO chemisorption on the surface consisted with the Fermi level shift observed in the STS experiments. Due to this electron transfer, the Fermi level of CuPc moves toward the valence band (HOMO). Although negative charge was transferred to the Au(111) surface, there is nearly negligible change of the Au(111) DOS in Figure 4(b). Au(111) has a very high density of free electrons; therefore, transferred the electrons do not induce noticeable changes in the Au(111) DOS consistent with a relatively high saturation coverage for NO/CuPc/Au(111).

DFT calculation shows NO form chemisorption sites on CuPc/graphene and the DOS of graphene is perturbed by NO

dx.doi.org/10.1021/jp5002258 | J. Phys. Chem. C 2014, 118, 10076−10082

chemisorption consistent with the low saturated coverage observed in Figure 3(d). As shown in Figure 4, parts (d)−(f) as well as SI Figure S3, the charge transfer is in the opposite direction for NO chemisorption on CuPc/graphene and CuPc/Au(111). Initially, HOPG donates 0.025 electrons per CuPc molecule to adsorbate-free CuPc; after NO chemisorption, HOPG donates an additional 0.025 electrons to both NO and reacted CuPc, and there is a corresponding decrease in the DOS of graphene at 1 eV below the Fermi surface in the valence band. It is noted that DFT calculations show NO adsorption on bare graphene has weak binding, 29 mV, and induces only small charge transfer (0.018 e); conversely, the binding of NO to CuPc/HOPG has stronger binding, 250 mV, and induces a charge transfer from HOPG of 0.025 e.[55] This means for 300 K sensing the coverage of NO would be many orders of magnitude greater for CuPc/HOPG than bare HOPG thereby increasing the sensor sensitivity. Furthermore, the CuPc/HOPG will be far more selective. Conversely, as shown in Figure 4(e), NO chemisorption induces an increase of the DOS in CuPc at −4.5 eV. It is noted although CuPc molecules accept electron charge from graphene during NO reaction, CuPc molecules also donates almost all (∼0.05 e) of its excess electrons to NO simultaneously, consistent with Fermi level shift observed in the STS experiments.

To confirm the experimental observation of low saturation coverage and the hypothesis of NO chemisorption inducing significant change in the graphene electronic structure, the effect of coverage upon NO binding on CuPc/graphene was calculated using a two CuPc molecules/graphene model, as shown in Figure 4d and SI Figure S3. The binding energy of initial NO chemisorbate on CuPc/HOPG is −0.24 eV, while the neighboring NO chemisorption site has only a −0.12 eV binding energy. This decrease of binding energy is consistent with a decreasing coverage, which results in small saturation NO coverage on HOPG. The low DOS of graphene both limits the saturation coverage of NO/CuPc/graphene and likely renders it to be an extremely sensitive chemical sensor. Because graphene has a low density of states, even small electronic perturbations can induce large sensitivity in sensors based on graphene.[6,7]

CONCLUSIONS

In order to elucidate chemisorption nature of NO with CuPc/HOPG, scanning tunneling microscopy (STM) was used to study NO dosed on CuPc monolayers deposited on Au(111) and HOPG. After saturating dosing of NO onto CuPc/Au(111), only, ∼7% of CuPc molecules form chemisorption sites with NO. STS shows that NO induces a Fermi level shift to from the middle of the band gap toward the valence band (HOMO). After dosing an equal amount of NO on CuPc/HOPG, NO forms only 0.1% chemisorption sites on CuPc/HOPG (70× lower than on CuPc/Au(111)), but the chemisorption sites and the Fermi level shift appear nearly identical for NO/CuPc/HOPG and NO/CuPc/Au. DFT calculations show that NO chemisorption with CuPc/Au(111) induces electron loss for NO and transfer to Au(111), but the density of states (DOS) of Au(111) shows negligible change, due to large DOS on Au. Conversely, for NO/CuPc/HOPG, negative charge is transferred from graphene to NO, and there is a large decrease of DOS in graphene around 1 eV below the Fermi surface in the valence band. This altered DOS of graphene induces a decreased binding energy for NO chemisorption in neighboring sites consistent with low saturation coverage. However, even though the saturation coverage of NO/CuPc/graphene is low, the electronic structure of graphene can be highly altered, because of the very low density of states of graphene. It is noted that NO adsorption on bare graphene has a very low binding energy (29 mV) compared to NO/CuPc/HOPG (250 mV).[55] Therefore, it can be expected that chemical sensors based NO/CuPc/graphene will have a few orders of magnitude higher sensitivity than that for NO/graphene bare sensors; in general, CuPc and other phthalocyanine functionalization can extend the reported sensitivity for bare graphene based sensors of highly reactive molecules (such as NO_2) to high sensitivity for a large range of modestly reactive molecules.[8] STM and DFT results show that functionalization of graphene with MPc would be a potential candidate for chemical sensing platforms, which can be expected to show high chemical sensitivity.

ASSOCIATED CONTENT

Supporting Information

Schematic diagram of STM and MBE chambers, charge density difference plots of NO/CuPc/Au(111), and NO/CuPc/HOPG. This material is available free of charge via the Internet at http://pubs.acs.org.

AUTHOR INFORMATION

Corresponding Author

*Phone: + 01-858-534-3368; e-mail: akummel@ucsd.edu.

Notes

The authors declare no competing financial interest.

ACKNOWLEDGMENTS

This work was supported by NSF Grant CHE-0848502 and by STARnet, a Semiconductor Research Corporation program, sponsored by MARCO and DARPA and by SRC NRI SWAN. DFT calculation work was also supported from NSF TeraGrid (XSEDE) resources under allocation numbers [TG-SEE090006], [TG-DMR110091], and [TG-DMR130127]. Use of the Center for Nanoscale Materials was supported by the US Department of Energy, Office of Science, Office of Basic Energy Sciences, under Contract No. DE-AC02-06CH11357.

REFERENCES

(1) Novoselov, K. S.; Geim, A. K.; Morozov, S. V.; Jiang, D.; Zhang, Y.; Dubonos, S. V.; Grigorieva, I. V.; Firsov, A. A. Electric Field Effect in Atomically Thin Carbon Films. *Science* **2004**, *306*, 666−669.

(2) Novoselov, K. S.; Geim, A. K.; Morozov, S. V.; Jiang, D.; Katsnelson, M. I.; Grigorieva, I. V.; Dubonos, S. V.; Firsov, A. A. Two-Dimensional Gas of Massless Dirac Fermions in Graphene. *Nature* **2005**, *438*, 197−200.

(3) Zhang, Y. B.; Tan, Y. W.; Stormer, H. L.; Kim, P. Experimental Observation of the Quantum Hall Effect and Berry's Phase in Graphene. *Nature* **2005**, *438*, 201−204.

(4) Fiori, G.; Iannaccone, G. Simulation of Graphene Nanoribbon Field-effect Transistors. *IEEE Electron Dev. Lett.* **2007**, *28*, 760−762.

(5) Lemme, M. C.; Echtermeyer, T. J.; Baus, M.; Kurz, H. A Graphene Field-Effect Device. *IEEE Electron Dev. Lett.* **2007**, *28*, 282−284.

(6) Hill, E. W.; Vijayaragahvan, A.; Novoselov, K. Graphene Sensors. *IEEE Sens J.* **2011**, *11*, 3161−3170.

(7) He, Q. Y.; Wu, S. X.; Yin, Z. Y.; Zhang, H. Graphene-Based Electronic Sensors. *Chem. Sci.* **2012**, *3*, 1764−1772.

(8) Schedin, F.; Geim, A. K.; Morozov, S. V.; Hill, E. W.; Blake, P.; Katsnelson, M. I.; Novoselov, K. S. Detection of Individual Gas Molecules Adsorbed on Graphene. *Nat. Mater.* **2007**, *6*, 652−655.

(9) Dan, Y. P.; Lu, Y.; Kybert, N. J.; Luo, Z. T.; Johnson, A. T. C. Intrinsic Response of Graphene Vapor Sensors. *Nano Lett.* **2009**, *9*, 1472−1475.
(10) Joshi, R. K.; Gomez, H.; Alvi, F.; Kumar, A. Graphene Films and Ribbons for Sensing of O-2, and 100 ppm of CO and NO_2 in Practical Conditions. *J. Phys. Chem. C* **2010**, *114*, 6610−6613.
(11) Schniepp, H. C.; Li, J. L.; McAllister, M. J.; Sai, H.; Herrera-Alonso, M.; Adamson, D. H.; Prud'homme, R. K.; Car, R.; Saville, D. A.; Aksay, I. A. Functionalized Single Graphene Sheets Derived From Splitting Graphite Oxide. *J. Phys. Chem. B* **2006**, *110*, 8535−8539.
(12) Stankovich, S.; Dikin, D. A.; Piner, R. D.; Kohlhaas, K. A.; Kleinhammes, A.; Jia, Y.; Wu, Y.; Nguyen, S. T.; Ruoff, R. S. Synthesis of Graphene-Based Nanosheets via Chemical Reduction of Exfoliated Graphite Oxide. *Carbon* **2007**, *45*, 1558−1565.
(13) Eda, G.; Fanchini, G.; Chhowalla, M. Large-area Ultrathin Films of Reduced Graphene Oxide as a Transparent and Flexible Electronic Material. *Nat. Nanotechnol.* **2008**, *3*, 270−274.
(14) Fang, Y. X.; Guo, S. J.; Zhu, C. Z.; Zhai, Y. M.; Wang, E. K. Self-Assembly of Cationic Polyelectrolyte-Functionalized Graphene Nanosheets and Gold Nanoparticles: A Two-Dimensional Heterostructure for Hydrogen Peroxide Sensing. *Langmuir* **2010**, *26*, 11277−11282.
(15) Luo, J.; Chen, Y. Z.; Ma, Q.; Liu, R.; Liu, X. Y. Layer-by-Layer Self-Assembled Hybrid Multilayer Films Based on Poly(sodium 4-styrenesulfonate) Stabilized Graphene with Polyaniline and their Electrochemical Sensing Properties. *RSC Adv.* **2013**, *3*, 17866−17873.
(16) Wang, Q. H.; Hersam, M. C. Room-temperature Molecular-resolution Characterization of Self-Assembled Organic Monolayers on Epitaxial Graphene. *Nat. Chem.* **2009**, *1*, 206−211.
(17) Wright, J. D. Gas-Adsorption on Phthalocyanines and Its Effects on Electrical-Properties. *Prog. Surf. Sci.* **1989**, *31*, 1−60.
(18) Archer, P. B. M.; Chadwick, A. V.; Miasik, J. J.; Tamizi, M.; Wright, J. D. Kinetic Factors in the Response of Organometallic Semiconductor Gas Sensors. *Sens. Actuators* **1989**, *16*, 379−392.
(19) Ho, K. C.; Tsou, Y. H. Chemiresistor-type NO Gas Sensor Based on Nickel Phthalocyanine Thin Films. *Sens. Actuators B-Chem.* **2001**, *77*, 253−259.
(20) van Faassen, E.; Kerp, H. Explanation of the Low Oxygen Sensitivity of Thin Film Phthalocyanine Gas Sensors. *Sens. Actuators B-Chem.* **2003**, *88*, 329−333.
(21) Bohrer, F. I.; Colesniuc, C. N.; Park, J.; Ruidiaz, M. E.; Schuller, I. K.; Kummel, A. C.; Trogler, W. C. Comparative Gas Sensing in Cobalt, Nickel, Copper, Zinc, and Metal-Free Phthalocyanine Chemiresistors. *J. Am. Chem. Soc.* **2009**, *131*, 478−485.
(22) Grate, J. W.; Klusty, M.; Barger, W. R.; Snow, A. W. Role of Selective Sorption in Chemiresistor Sensors for Organophosphorus Detection. *Anal. Chem.* **1990**, *62*, 1927−1934.
(23) Ludwig, C.; Strohmaier, R.; Petersen, J.; Gompf, B.; Eisenmenger, W. Epitaxy and Scanning-Tunneling-Microscopy Image-Contrast of Copper Phthalocyanine on Graphite and Mos2. *J. Vac Sci. Technol. B* **1994**, *12*, 1963−1966.
(24) Lu, X.; Hipps, K. W.; Wang, X. D.; Mazur, U. Scanning Tunneling microscopy of Metal Phthalocyanines: d(7) and d(9) Cases. *J. Am. Chem. Soc.* **1996**, *118*, 7197−7202.
(25) Lu, X.; Hipps, K. W. Scanning Tunneling Microscopy of Metal Phthalocyanines: d(6) and d(8) Cases. *J. Phys. Chem. B* **1997**, *101*, 5391−5396.
(26) Nilson, K.; Ahlund, J.; Brena, B.; Gothelid, E.; Schiessling, J.; Martensson, N.; Puglia, C. Scanning Tunneling Microscopy Study of Metal-Free Phthalocyanine Monolayer Structures on Graphite. *J. Chem. Phys.* **2007**, *127*.
(27) Wang, Y. F.; Kroger, J.; Berndt, R.; Hofer, W. Structural and Electronic Properties of Ultrathin Tin-Phthalocyanine Films on Ag(111) at the Single-Molecule Level. *Angew. Chem., Int. Ed.* **2009**, *48*, 1261−1265.
(28) Eley, D. D.; Hazeldin, Dj; Palmer, T. F. Mass-Spectra, Ionization-Potentials and Related Properties of Metal-Free and Transition-Metal Phthalocyanines. *J. Chem. Soc. Faraday Trans. 2* **1973**, *69*, 1808−1814.
(29) Tegeler, E.; Iwan, M.; Koch, E. E. Electronic-Structure of the Valence Bands of H-2-Phthalocyanine, Mg-Phthalocyanine and Pt-Phthalocyanine Derived from Soft-X-Ray Emission and Photoelectron Emission-Spectra. *J. Electron. Spectrosc.* **1981**, *22*, 297−307.
(30) Martin, M.; Andre, J. J.; Simon, J. Influence of Dioxygen on the Junction Properties of Metallophthalocyanine Based Devices. *J. Appl. Phys.* **1983**, *54*, 2792−2794.
(31) Kerp, H. R.; Westerduin, K. T.; van Veen, A. T.; van Faassen, E. E. Quantification and Effects of Molecular Oxygen and Water in Zinc Phthalocyanine Layers. *J. Mater. Res.* **2001**, *16*, 503−511.
(32) Simon, J.; André, J. J.; Lehn, J. M.; Rees, C. W. *Molecular Semiconductors: Photoelectrical Properties and Solar Cells*; Springer-Verlag: Berlin/New York, 1985; pp 79−149.
(33) Buchholz, J. C.; Somorjai, G. A. Surface-Structures of Phthalocyanine Monolayers and Vapor-Grown Films—Low-Energy Electron-Diffraction Study. *J. Chem. Phys.* **1977**, *66*, 573−580.
(34) Arumainayagam, C. R.; Madix, R. J. Molecular-Beam Studies of Gas-Surface Collision Dynamics. *Prog. Surf. Sci.* **1991**, *38*, 1−102.
(35) Nguyen, T. Q.; Escano, M. C. S.; Kasai, H. Nitric Oxide Adsorption Effects on Metal Phthalocyanines. *J. Phys. Chem. B* **2010**, *114*, 10017−10021.
(36) Hill, I. G.; Kahn, A.; Soos, Z. G.; Pascal, R. A. Charge-separation Energy in Films of π-Conjugated Organic Molecules. *Chem. Phys. Lett.* **2000**, *327*, 181−188.
(37) Schwieger, T.; Peisert, H.; Golden, M. S.; Knupfer, M.; Fink, J. Electronic Structure of the Organic Semiconductor Copper Phthalocyanine and K-CuPc Studied Using Photoemission Spectroscopy. *Phys. Rev. B* **2002**, *66*.
(38) Soe, W. H.; Manzano, C.; De Sarkar, A.; Chandrasekhar, N.; Joachim, C. Direct Observation of Molecular Orbitals of Pentacene Physisorbed on Au(111) by Scanning Tunneling Microscope. *Phys. Rev. Lett.* **2009**, *102*.
(39) Yan, L.; Watkins, N. J.; Zorba, S.; Gao, Y. L.; Tang, C. W. Thermodynamic Equilibrium and Metal-Organic Interface Dipole. *Appl. Phys. Lett.* **2002**, *81*, 2752−2754.
(40) Chen, W.; Wang, L.; Qi, D. C.; Chen, S.; Gao, X. Y.; Wee, A. T. S. Probing the Ultrafast Electron Transfer at the CuPc/Au(111) Interface. *Appl. Phys. Lett.* **2006**, *88*.
(41) Hu, Z. P.; Li, B.; Zhao, A. D.; Yang, J. L.; Hou, J. G. Electronic and Magnetic Properties of Metal Phthalocyanines on Au(111) Surface: A First-Principles Study. *J. Phys. Chem. C* **2008**, *112*, 13650−13655.
(42) Zhang, Y. Y.; Du, S. X.; Gao, H. J. Binding Configuration, Electronic Structure, and Magnetic Properties of Metal Phthalocyanines on a Au(111) Surface Studied with Ab Initio Calculations. *Phys. Rev. B* **2011**, *84*.
(43) Schaffer, A. M.; Gouterma, M.; Davidson, E. R. Porphyrins 0.28. Extended Huckel Calculations on Metal Phthalocyanines and Tetrazaporphins. *Theor. Chim. Acta* **1973**, *30*, 9−30.
(44) Figgis, B. N.; Kucharski, E. S.; Reynolds, P. A. Electronic-Structure of Cobalt Phthalocyanine—A Charge-Density Study. *J. Am. Chem. Soc.* **1989**, *111*, 1683−1692.
(45) Kera, S.; Yamane, H.; Sakuragi, I.; Okudaira, K. K.; Ueno, N. Very Narrow Photoemission Bandwidth of the Highest Occupied State in a Copper-Phthalocyanine Monolayer. *Chem. Phys. Lett.* **2002**, *364*, 93−98.
(46) Shimada, T.; Hamaguchi, K.; Koma, A.; Ohuchi, F. S. Electronic Structures at the Interfaces between Copper Phthalocyanine and Layered Materials. *Appl. Phys. Lett.* **1998**, *72*, 1869−1871.
(47) Komolov, A. S.; M?ller, P. J. Unoccupied Electronic States and Energy Level Alignment at Interfaces Between Cu-phthalocyanine Films and Semiconductor Surfaces. *Synth. Met.* **2003**, *138*, 119−123.
(48) Kera, S.; Yabuuchi, Y.; Yamane, H.; Setoyama, H.; Okudaira, K. K.; Kahn, A.; Ueno, N. Impact of an Interface Dipole Layer on Molecular Level Alignment at an Organic-Conductor Interface Studied by Ultraviolet Photoemission Spectroscopy. *Phys. Rev. B* **2004**, *70*.
(49) Ren, J.; Meng, S.; Wang, Y. L.; Ma, X. C.; Xue, Q. K.; Kaxiras, E. Properties of Copper (fluoro-)phthalocyanine Layers Deposited on Epitaxial Graphene. *J. Chem. Phys.* **2011**, *134*.

(50) Kresse, G.; Hafner, J. Abinitio Molecular-Dynamics for Liquid-Metals. *Phys. Rev. B* **1993**, *47*, 558−561.
(51) Kresse, G.; Furthmuller, J. Efficient Iterative Schemes for Ab Initio Total-energy Calculations Using a Alane-wave Basis set. *Phys. Rev. B* **1996**, *54*, 11169−11186.
(52) Kresse, G.; Furthmuller, J. Efficiency of ab-Initio Total Energy Calculations for Metals and Semiconductors Using a Plane-Wave Basis Set. *Comput. Mater. Sci.* **1996**, *6*, 15−50.
(53) Grimme, S. Semiempirical GGA-Type Density Functional Constructed with a Long-Range Dispersion Correction. *J. Comput. Chem.* **2006**, *27*, 1787−1799.
(54) Tkatchenko, A.; Scheffler, M. Accurate Molecular Van Der Waals Interactions from Ground-State Electron Density and Free-Atom Reference Data. *Phys. Rev. Lett.* **2009**, *102*.
(55) Leenaerts, O.; Partoens, B.; Peeters, F. M. Adsorption of $H_{(2)}O$, $NH_{(3)}$, CO, $NO_{(2)}$, and NO on Graphene: A First-Principles Study. *Phys. Rev. B* **2008**, *77*.